Cambridge Centre for Computational Chemical Engineering

University of Cambridge

Department of Chemical Engineering

Preprint ISSN 1473 – 4273

New polycyclic aromatic hydrocarbon (PAH) surface processes to improve the model prediction of the composition of combustion-generated PAHs and soot

Abhijeet Raj, Peter Man, Tim Totton, Markus Sander,

Raphael Shirley, Markus Kraft *

released: 30 March 2009

Department of Chemical Engineering and Biotechnology
University of Cambridge
New Museums Site
Pembroke Street
Cambridge, CB2 3RA
UK
*E-mail: mk306@cam.ac.uk

Preprint No. 69

c4e

Key words and phrases: DFT, PAH, soot, aromatic site, kinetic Monte-Carlo, simulation, modelling

Edited by
Cambridge Centre for Computational Chemical Engineering
Department of Chemical Engineering
University of Cambridge
Cambridge CB2 3RA
United Kingdom.

Fax: + 44 (0)1223 334796
E-Mail: c4e@cheng.cam.ac.uk
World Wide Web: http://www.cheng.cam.ac.uk/c4e/

Abstract

Two new polycyclic aromatic hydrocarbon (PAH) surface processes are proposed, which can cause dehydrogenation and "rounding" of PAH molecules. The reaction pathways for both the processes involve decyclisation of a 6-member ring present on the PAH surface. 1,6-hydrogen migration in the bay region formed by nearby carbon atoms provides an alternate route for both the processes to proceed. The energetics and kinetics of the proposed processes are investigated using density functional theory and transition state theory, respectively. The B3LYP functional with the 6-311++G(d,p) basis set is employed for the geometry optimisation and vibrational frequency analysis of the chemical species and the transition states. The current PAH growth mechanism is extended by including the new processes. A detailed PAH growth model, the kinetic Monte Carlo—aromatic site (KMC-ARS) model [Raj *et al.*, Combust. Flame, 156:896-913, 2009] is used to study PAH growth with the extended mechanism. Computed ensembles are generated for large PAHs present in a C_2H_2 flame with 70–320 carbon atoms, and are compared to the experimentally observed ensembles. The inclusion of the new PAH processes in the chemical mechanism is found to improve the predicted composition of the large PAH molecules, especially for the PAHs with 70–200 carbon atoms.

Contents

1 Introduction **3**

2 Calculation details **4**

3 Reaction pathways **7**

3.1 PAH Process 1 7

3.2 PAH Process 2 9

4 Kinetic Monte Carlo–Aromatic Site (KMC-ARS) Model **10**

5 Results and discussion **13**

5.1 Reaction rates 13

5.2 KMC simulation 15

5.3 Sensitivity analysis 20

5.3.1 Hypothesis test 22

6 Conclusion **22**

1 Introduction

Soot particles and polycyclic aromatic hydrocarbons (PAHs) are considered to be the major pollutants, generated from combustion devices such as flames and engines [32]. A number of human diseases such as cancer and asthma are associated with them [4]. In order to reduce the production of these substances, it is important to gain an insight into their formation and growth pathways [21]. In the last few decades, several theoretical and experimental investigations have been conducted in these directions. In [10, 22, 37, 38], morphological studies were conducted on soot particles by observing their High Resolution Transmission Electron Microscopy (HRTEM) images. These studies revealed that soot particles exhibit microcrystallinity near the outer edge. This crystallinity arises due to stacking of planar PAHs to form parallel atomic layers and their alignment along the periphery of soot particles. The recent experimental findings of Vander Wal *et al.* [39] indicate the amorphous nature of soot nuclei due to the presence of randomly oriented PAHs [39]. It can be concluded from these studies that PAH molecules act as a soot precursor, and therefore, to study the soot formation process, knowledge about the formation and growth of PAHs is required.

To facilitate the study of the growth of PAH molecules, a detailed chemical mechanism, involving a large number of PAH processes, is available in the literature based on the gaseous species present in abundance in combustion devices such as $\mathrm{C_2H_2}$ and small aromatic compounds such as benzene and naphthalene [16, 30, 46, 47]. The rate constants of the elementary reactions involved in the processes have been derived theoretically [15, 43, 44]. Recently, a number of models have been proposed to study PAH growth in flame environments based on the detailed PAH mechanism [16, 30, 40]. The PAH growth model presented by Violi [40] models large, non-planar PAH sheets in a flame-like environment. A large set of reactions describe the growth of a PAH molecule, using a kinetic Monte Carlo (KMC) algorithm. Molecular dynamics (MD) calculations [40] are used to optimise the PAH geometry. Another PAH model, the kinetic Monte Carlo—aromatic site (KMC-ARS) model, is proposed in our previous work [30], in which a single planar PAH molecule is simulated using a kinetic Monte Carlo algorithm. In that work [30], a detailed study on the variation in PAH characteristics with flame environments was conducted. It was shown through the KMC simulations that the present reaction mechanism predicts, reasonably well, the ensembles of the PAHs observed in different flame environments [23, 45]. The comparison between the computed and the observed PAH ensembles was carried out on C-H diagrams, on which each PAH molecule with a molecule formula $\mathrm{C_xH_y}$ is represented as a data point (x, y). In the simulations, some H-rich PAH molecules are predicted at higher heights above the burner (HABs), than are observed experimentally. The experimentally observed PAHs at higher HABs mostly contain peri-condensed rings (H-poor PAHs). Weilmünster *et al.* [45] conducted an experimental study on PAHs present in an aliphatic flame, and suggested that, at higher HABs, the PAH growth rate decreases due to decrease in the concentration of chemical species like $\mathrm{C_2H_2}$. At such points, processes involving PAH rearrangement and ring desorption mainly take place. These processes cause dehydrogenation and "rounding" of PAHs, and therefore are required to be included in the PAH growth mechanism.

In the recent past, a comprehensive model for soot formation and growth, named as,

the aromatic site counting – primary particle (ARSC-PP) model [7] has been developed. This model is based on the assumption that a soot particle is formed from planar PAH molecules. The growth of PAHs present in soot takes place via a detailed chemical mechanism, which is similar to the one used for the KMC-ARS model. The ARSC-PP model is able to track the size of spherical nanostructures (primary particles) forming chain-like aggregate structure of soot, and, therefore, is more detailed as compared to the previously proposed surface-volume soot model [29]. With this model, it is possible to obtain information about the composition (in terms of the number of C and H atoms) and the size distributions of soot particles in combustion devices [33, 34], and produce representative TEM-like images of soot particles [9]. With the current reaction mechanism, the ARSC-PP model under-predicts the C/H ratio of soot particles [9]. This indicates that the present mechanism for soot (or PAH) growth requires some dehydrogenation processes to improve the model predictions of soot composition in combustion devices.

The aim of this paper is to extend the detailed PAH growth mechanism by including two new PAH rearrangement and ring desorption processes. Two highly competitive routes for each process have been suggested. A theoretical study has been conducted using density functional theory (DFT) and transition state theory (TST) to determine the rates for the elementary reactions involved in the suggested processes. The calculated rate constants have been corrected to account for the quantum tunnelling effect. The evaluated rate for the ring decyclisation reaction–a principal reaction in both the proposed pathways has been compared to the rates for this reaction given in the literature. Furthermore, the KMC-ARS model has been used along with the extended PAH growth mechanism to study the effect of the inclusion of the new processes on the composition of computed PAHs in a C_2H_2 flame. Finally, a sensitivity analysis has been carried out by varying the rate constants of all the elementary reaction involved in the PAH growth mechanism to study its effect on the computed results by the KMC-ARS model.

2 Calculation details

The molecular structures of the stable chemical species and transition states involved in the proposed PAH processes were optimised using the B3LYP hybrid functional and the 6-311++G(d,p) basis set. For the stable species, the structures were optimised with different spin multiplicities to determine the multiplicity with the minimum energy and reasonable geometry. All the DFT calculations were performed using Gaussian 03 [17].

Before employing B3LYP/6-311++G(d,p) for the theoretical calculations in this work, a number of experimental validations were carried out by comparing the experimental data available for carbon-hydrogen systems with the calculated values. The bond dissociation energy of the C-H bond in benzene was determined using B3LYP/6-311++G(d,p), and was found to be 110.9 kcal/mol. This value agrees reasonably well with the experimental C-H bond dissociation energies of 113.9, 109.3 and 102.1 kcal/mol provided in Gribov *et al.* [19] and refs. therein, and a recent value of 112.9 $\pm$ 0.5 kcal/mol given in [26]. The more accurate (and substantially slower) second-order Møller-Plesset perturbation theory, MP2/6-31G(d,p) is shown to predict a BDE of 117.7 kcal/mol in [19]. The PAH processes proposed in this work require an abstraction of an H atom present

on the PAH for initiation. Therefore, the B3LYP functional was used to study the H-abstraction process on different hydrocarbons, for which experimentally determined reaction energies and barrier heights were available. For methane H-abstraction reaction ($CH_4 + H \rightarrow CH_3 + H_2$), B3LYP/6-311++G(d,p) predicts the reaction energy and barrier height to be 0.94 and 9.54 kcal/mol, respectively, which compare reasonably well with the experimental values of 0.6 and 11.9 kcal/mol [5, 27, 36]. The "gold-standard" coupled-cluster singles, doubles and perturbative triples, CCSD(T)/AUG-cc-pVQZ predicts the barrier height for this reaction as 14.9 kcal/mol [48]. A similar calculation was done for benzene H-abstraction reaction ($C_6H_6 + H \rightarrow C_6H_5 + H_2$). The reaction energy and the barrier height calculated with B3LYP/6-311++G(d,p) were 7.28 and 12.2 kcal/mol, respectively. In [28], these energies were determined by performing single point energy calculations using RCCSD(T)/6-31G(d,p) on the geometries optimised using MP2/6-31G(d), and were found to be 11.8 and 22.3 kcal/mol, respectively. An experimental investigation on this reaction reports its reaction energy as 8.95 kcal/mol [5]. It is clear from the above comparisons and similar comparisons in the literature [24, 28, 35, 36] that the B3LYP functional under-predicts the reaction barrier heights. This under-prediction can lead to an overestimation of the reaction rate constants. According to the findings of [46] and refs. therein, the error in the calculated reaction barrier introduced by density functional theory (DFT) can be as high as 5 kcal/mol. Figure 1 shows the effect of uncertainty in reaction barrier height (activation energy) on the rate constant, assuming it to be in the modified Arrhenius form (equation 1).

$$k(T) = A \times T^n \times \exp\left(\frac{-E}{RT}\right) \tag{1}$$

It is clear from this figure that, for T $>$ 1000 K, the change in the rate constant remains within an order of magnitude, even when $\Delta E = 5$ kcal/mol. However, at lower temperatures ($\approx$300 K), an under-prediction in the barrier height by 5 kcal/mol can over-predict the rate constant by more than three orders of magnitude. Therefore, a large error in the reaction barrier is not permissible at low temperatures. A further inaccuracy in the quantum calculations can arise due to spin contamination in open shell systems. Spin contamination can significantly affect the energy, geometry and calculated spin density of the molecules [49]. The expectation value of the spin operator $\hat{S}^2$, $\langle S^2 \rangle$ gives a measure of the amount of spin contamination introduced by a given level of theory. If there is no spin contamination, $\langle S^2 \rangle$ should be equal to $s(s+1)$, where s equals half the number of unpaired electrons. In [3, 35], it is shown by observing $\langle S^2 \rangle$ for a number of stable species and transition states that DFT introduces a negligible amount of spin contamination, and so does CCSD(T). The values of $\langle S^2 \rangle$ for all the chemical species and transition states involved in the proposed processes are shown later in this paper.

To assure that the inaccuracy in the quantum calculations performed using DFT is not very high, a higher level of theory such as CCSD(T), which is believed to predict the reaction barrier very well with negligible amount of spin contamination, can be employed for such calculations on a given molecular system. However, with the present computing resources, such a high level calculation can only be done for small molecules in a reasonable computational time. For large molecules such as PAHs, DFT is considered to be a standard choice, as it is computationally much cheaper than higher levels of theory. We hope to address, in future work, the deficiencies such as under-predicted barrier heights

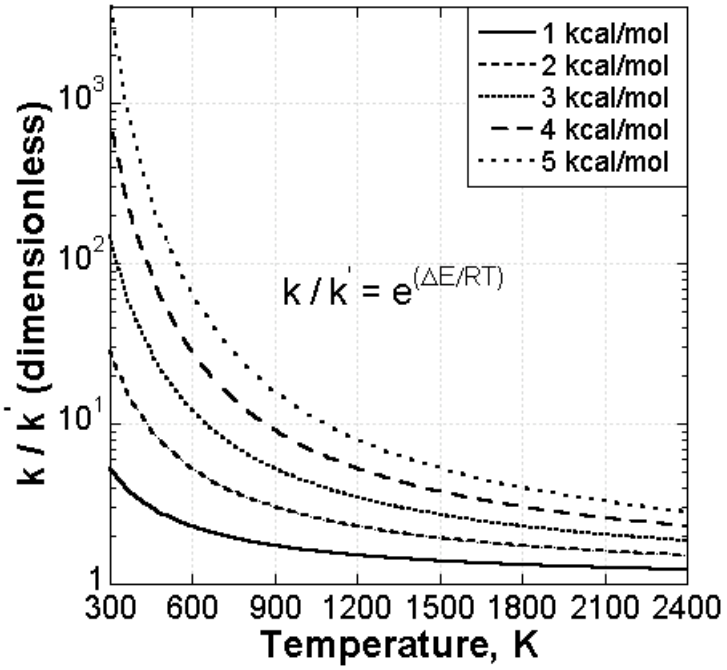

Figure 1: *Effect of change in activation energy on the reaction rate constant. ΔE represents the error in evaluated reaction barrier height (activation energy), E. k and k' are the rate constants with activation energies E and E+ΔE, respectively.*

with B3LYP by considering some recent developments in functionals such as M06 [50] or rCAM-B3LYP [12] which give improved barrier heights. Since the PAH processes mainly take place at higher temperatures, DFT can provide a reasonable estimate of the reaction rate constants with an accuracy within an order of magnitude. Experimental investigations on the barrier heights of PAH reactions will be very useful to understand the systematic errors in quantum calculations.

The rate constants for the reactions involved in the proposed processes were evaluated using transition state theory (TST). The partition functions for the transition state and reactants were calculated at a range of temperatures (300–3000 K) using the vibrational frequencies, moments of inertia, mass and electronic multiplicity, all of which are given by the quantum calculations. A linear least-square fitting algorithm was used to fit the modified Arrhenius expression (equation 1) to the data points of the rate constants in order to obtain the rate coefficients A, n and E. It is well known that the transition state theory, employed for the calculation of rate constants, does not consider the quantum tunnelling effect. This may lead to an under-estimation of the rate constants for the elementary reactions. To assess the role of quantum tunnelling, in the literature, there are four efficient methods to evaluate the tunnelling correction factor (or, transmission constant): Wigner correction, Eckwart correction, Zero-curvature tunnelling (ZCT) correction, small curvature tunnelling (SCT) correction. The first two one-dimensional methods are mainly used for the rates calculated using TST. The curvature tunnelling methods are generally used for the rates calculated using variational transition state theory (VTST). ZCT and SCT

predict the correction factor very efficiently, especially at low temperatures (T $<$ 500 K). However, at higher temperatures (T $>$ 500 K), the correction factors determined by all the methods begin to converge to similar values [6, 18]. In this work, the Wigner method was employed to obtain the tunnelling correction factors for all the elementary reactions. This correction factor, $C_W(T)$ is expressed as:

$$C_W(T) = 1 - \frac{1}{24}\left(\frac{h\nu^{\ddagger}}{k_B T}\right)^2 \tag{2}$$

where, h is Planck′s constant, k_B is Boltzmann constant, and $\nu^{\ddagger}$ is the imaginary frequency of the transition state. The rate constants are then evaluated as a product of $C_W(T)$ and $k(T)$.

3 Reaction pathways

This section details the elementary reaction steps involved in the two PAH processes proposed in this work. Both the processes require the presence of a 6-member ring adjacent to a bay site (a combined functional site [30]) to take place. To reduce the computational expense for quantum calculations, the smallest substrate molecule fulfilling the above requirement, benzo[c]phenanthrene was chosen as the parent molecular structure.

3.1 PAH Process 1

Figure 2 shows the potential energy diagram for the conversion of benzo[c]phenanthrene to pyrene. The reaction is initiated by the abstraction of an H atom present in the bay region of CS1. The abstraction process reduces the steric congestion in CS2. This was evident from the optimised geometries of CS1 and CS2. The 3D geometry of CS1 caused by the repulsion between the nearby H atoms in the bay region was lost, and CS2 gained a planar geometry, as observed in [41]. The structural stabilisation of CS2 leads to a lower reaction energy of 1.09 kcal/mol for this H-abstraction process, as compared to benzene H-abstraction reaction, which involves a reaction energy of 7.28 kcal/mol (see section 2). The next step involves the breakage of a 6-member ring near the bay region (decyclisation reaction). This reaction requires a potential energy barrier of 65.81 kcal/mol to be overcome. A similar ring-breakage mechanism has been proposed in [16] for the PAH processes involving conversion of a 6-member ring to a 5-member ring, and 6-member ring desorption. After the decyclisation of a 6-member ring, three possibilities can arise: (a) desorption of one of the aliphatic chains, (b) recombination of the aliphatic chains to form a 6-member ring, and (c) formation of cyclopentadienylidenecarbene type structure (with only one radical) by the two aliphatic chains. The possibilities (a) and (c) form the basis for the two PAH processes proposed in this work. In process 1, the desorption of a C_2H_2 molecule can take place via two routes–one involving the mediation of a H atom, and the other involving direct desorption of C_2H_2. The H-mediated desorption of C_2H_2 has been suggested in [16] by simultaneous addition and removal of an H atom and a

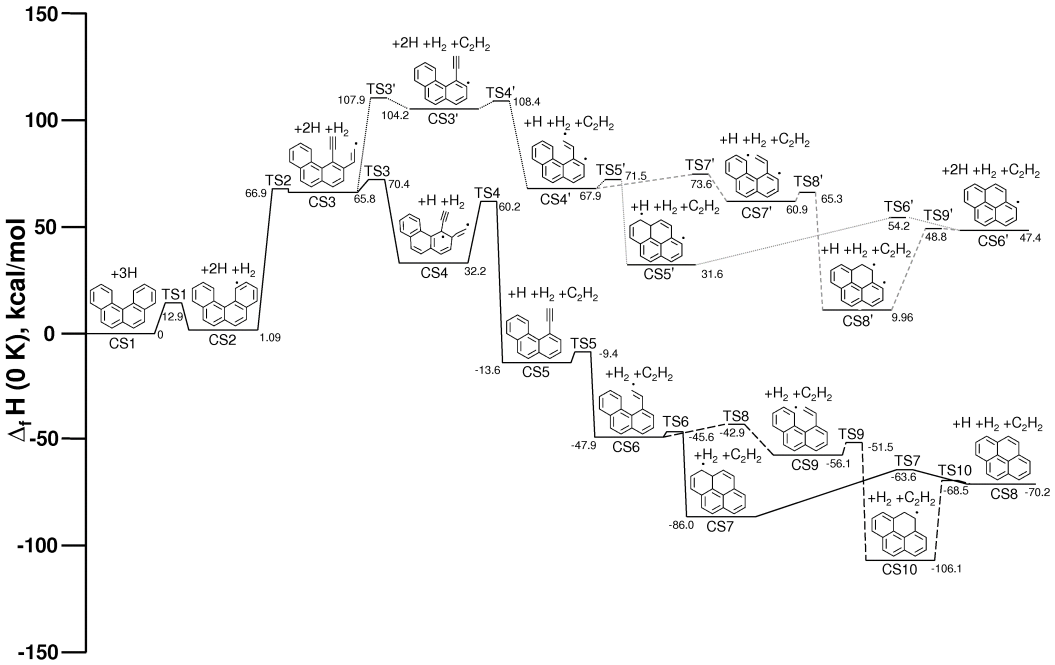

Figure 2: *Potential energy diagram showing energies of the chemical species (CS) and transition states (TS) involved in the conversion of benzo[c]phenanthrene to pyrene at 0 K. After the formation of CS6, two probable routes are shown here by solid and broken lines. Similarly, after the formation of CS4′, two probable routes are shown by dotted and broken lines.*

C_2H_2 molecule, respectively, as shown below:

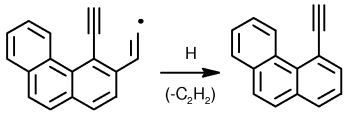

(3)

For this route, a negative reaction barrier was found. A further analysis of this pathway led to the conclusion that a stable molecule, CS4 gets formed by the addition of an H atom on CS3. The reaction CS3 $+\mathrm{H} \rightarrow$ CS4 involves a barrier of 4.6 kcal/mol. The desorption of a C_2H_2 molecule can then take place from CS4 to form CS5. Figure 3 shows the structures of the chemical species and the transition states involved in this route. After the formation of CS5, the principal reactions, that take place are H addition, H shift between the C atoms forming a bay site, bond formation between nearby C atoms, and removal of an H atom (from CS7 or CS10) to regain aromaticity, as shown in figure 2. The direct removal of C_2H_2 from CS3 can form CS3′, which requires an energy barrier of 42.1 kcal/mol to be overcome. Once CS3′ is formed, it can lead to the formation of a pyrene radical by following the same routes as CS5, as shown in figure 2.

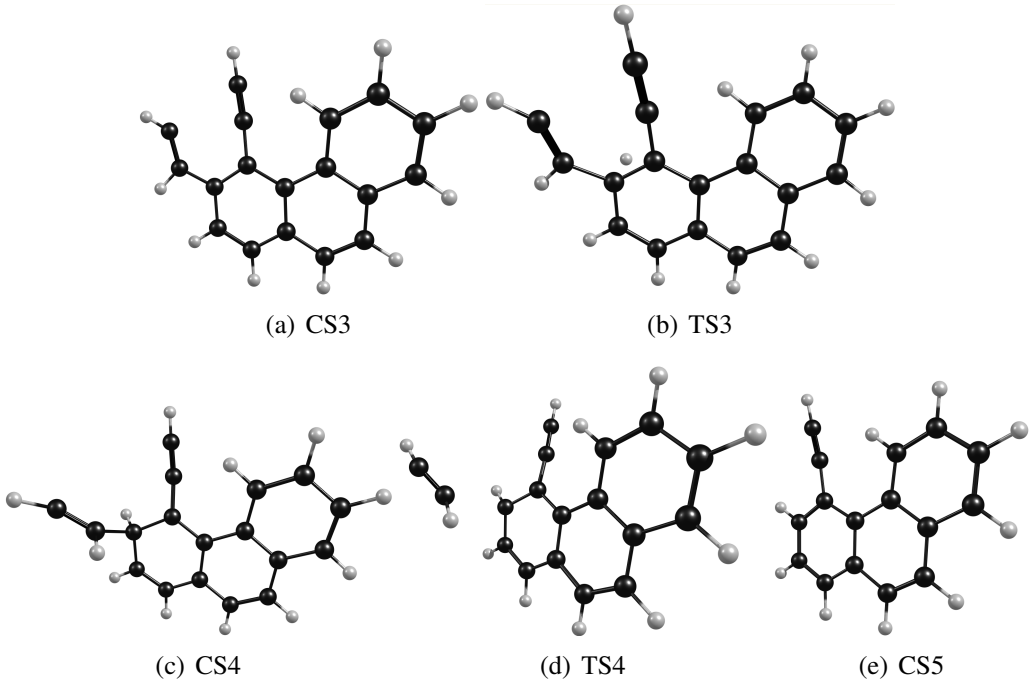

(a) CS3 (b) TS3

(c) CS4 (d) TS4 (e) CS5

Figure 3: *Structures of the chemical species and transition states involved in the conversion of CS3 → CS5.*

3.2 PAH Process 2

Figure 4 shows the potential energies of the chemical species and the transition states involved in the conversion of benzo[*c*]phenanthrene to cyclopenta[*cd*]pyrene relative to the starting species: CS1 and two H atoms. This process involves dehydrogenation of a PAH molecule through ring rearrangement. Similar to process 1, it initiates with the abstraction of an H atom and decyclisation of a 6-member ring. This decyclisation is followed by the formation of cyclopentadienylidenecarbene type structure (CS3 → CS11). For this reaction, a potential energy of only 4.3 kcal/mol is required, which is comparable to the energy barrier of 4.6 kcal/mol required for the reaction CS3 → CS4. This implies that both the pathways proposed in this work are highly competitive. After the formation of CS11, reactions involving C-C bond formation, H-shift and H-removal to regain aromaticity primarily take place. In [41], a different pathway for process 2 has been proposed, in which the reaction proceeds without the opening of a 6-member ring. This is detailed in section 5.

Most of the species involved in both the pathways have radical sites on them, and therefore, unrestricted DFT calculations were performed on such open-shell systems. To evaluate the amount of spin contamination introduced by DFT, $\langle S^2 \rangle$ values were found for all the chemical species and the transition states, and are shown in Table 1. For organic molecule calculations, the spin contamination is negligible if the value of $\langle S^2 \rangle$ differs from $s(s+1)$ by less than 10% [49]. It is clear from this table that the amount of spin contamination introduced by DFT is negligible for our molecular system.

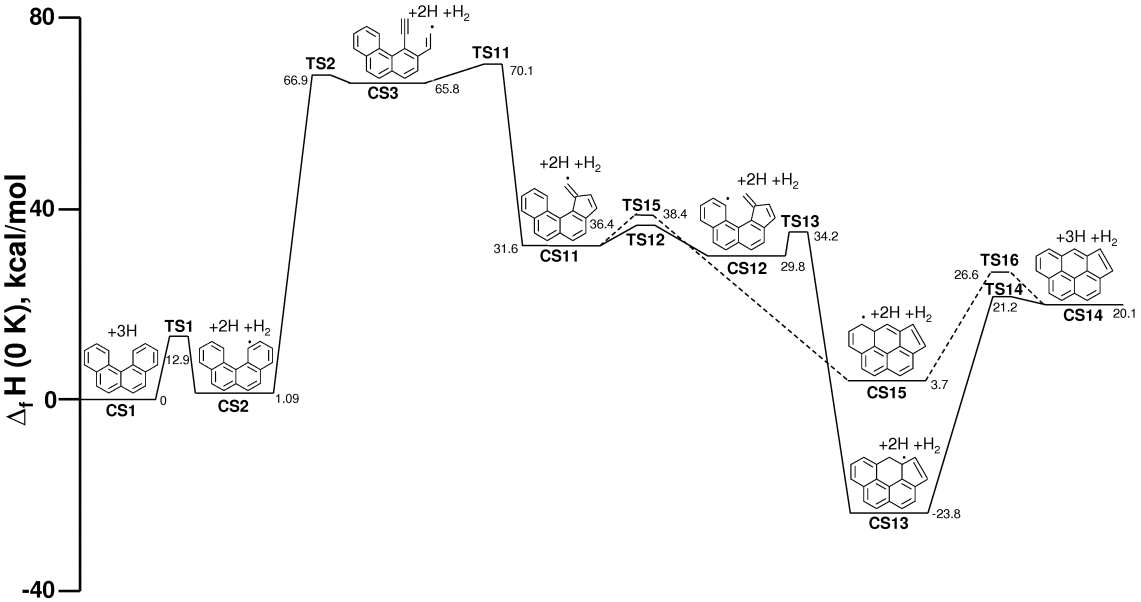

Figure 4: *Potential energy diagram showing energies of the chemical species (CS) and transition states (TS) involved in the conversion of benzo[c]phenanthrene to cyclopenta[cd]pyrene at 0 K. Two probable routes are shown here by solid and broken lines.*

As mentioned before, along with the processes proposed in this work, several other surface processes are present in the literature that can take place on a PAH molecule. A PAH process takes place on a particular type of functional site present on the PAH surface [8, 30]. The required type of site can be: a) an elementary site [30] (for example, a free-edge growth reaction requires a free-edge to take place), or b) a combined site [30] (for example, processes 1 and 2 require a 6-member ring adjacent to a bay site to take place). Therefore, the occurrence of a PAH process depends on the availability of the functional sites of particular types. After each surface reaction, the morphology of the PAH molecules changes, as a number of functional sites of different types are created and destroyed, simultaneously. This affects the rates of all the surface processes taking place [8, 30, 31]. In order to evaluate their rates after each reaction on a PAH, it is necessary to update the PAH structure after the reaction. Section 4 describes a model, which can simulate the growth of a PAH molecule and track its evolving structure.

4 Kinetic Monte Carlo–Aromatic Site (KMC-ARS) Model

A detailed PAH growth model, named as the KMC-ARS model, has been successfully applied to study the growth of a single PAH molecule in our previous studies [8, 30]. This section briefly summarises the main features of the model. The KMC-ARS model describes a PAH molecule in terms of the number of reactive sites present along its outer edge. Figure 5 shows an example PAH molecule with different types of sites [30]: free-edges, zig-zags, armchairs, bays, and five-membered rings.

Table 1: *$\langle S^2 \rangle$ for the species involved in pathways 1 and 2 obtained using B3LYP/6-311++G(d,p) level of theory. For singlet, doublet and triplet states, $\langle S^2 \rangle$ should be 0, 0.75 and 2, respectively. The number in the bracket shows the spin multiplicity.*

Chemical species	$\langle S^2 \rangle$	Chemical species	$\langle S^2 \rangle$	Transition states	$\langle S^2 \rangle$	Transition states	$\langle S^2 \rangle$
CS1 (1)	0	CS2 (2)	0.759	TS1 (2)	0.762	TS2 (2)	0.771
CS3 (2)	0.764	CS4 (3)	2.051	TS3 (3)	2.029	TS4 (3)	2.052
CS5 (1)	0	CS6 (2)	0.761	TS5 (2)	0.767	TS6 (2)	0.788
CS7 (2)	0.788	CS8 (1)	0	TS7 (2)	0.782	TS8 (2)	0.762
CS9 (2)	0.759	CS10 (2)	0.786	TS9 (2)	0.775	TS10 (2)	0.772
CS3′(2)	0.759	CS4′(3)	2.014	TS3′ (2)	0.772	TS4′ (3)	2.019
CS5′(3)	2.033	CS6′(2)	0.761	TS5′ (3)	2.034	TS6′ (3)	2.026
CS7′(3)	2.019	CS8′(3)	2.053	TS7′ (3)	2.042	TS8′ (3)	2.041
CS11 (2)	0.767	CS12 (2)	0.758	TS9′ (3)	2.041	TS11 (2)	0.777
CS13 (2)	0.767	CS14 (1)	0	TS12 (2)	0.764	TS13 (2)	0.798
CS15 (2)	0.787			TS14 (2)	0.767	TS15 (2)	0.796
				TS16 (2)	0.783		

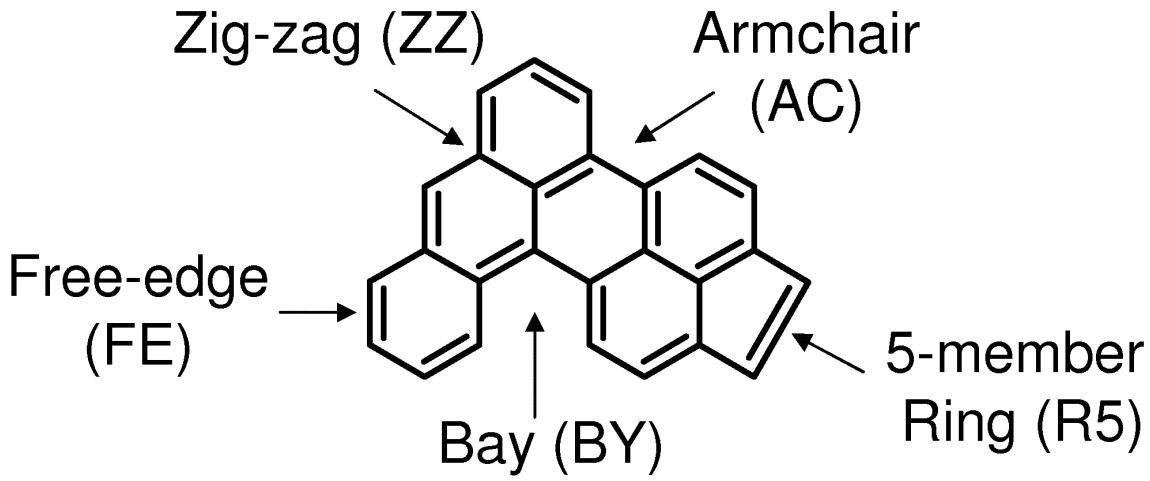

Figure 5: *An example PAH showing the principal surface site types.*

This model utilises a kinetic Monte Carlo algorithm along with a detailed chemical mechanism to simulate the growth of a PAH molecule. A list containing 17 PAH processes involved in the chemical mechanism is provided in [30]. This list has been extended in this work by including 3 more processes as shown in table 2.

Table 2: *New PAH reactions along with the jump processes and the process rates obtained after steady-state analysis [8, 30]. The reaction steps S1–S17 are provided in [30].*

Steps [Ref.]	Parent site
S18 6-member ring desorption at bay (Process 1)	**6-member ring next to bay**
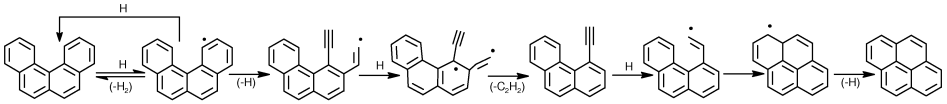	
Jump Process: 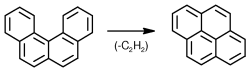	Rate: $k_{2a}\left(\frac{k_{1a}[\mathrm{H}]+k_{24}[\mathrm{OH}]}{k_{-1}[\mathrm{H_2}]+k_{25}[\mathrm{H}]+k_{-24}[\mathrm{H_2O}]+k_{2a}}\right)[\mathrm{C_{bay}R6}]$
S19 6-member ring rearrangement at bay (Process 2)	**6-member ring next to bay**
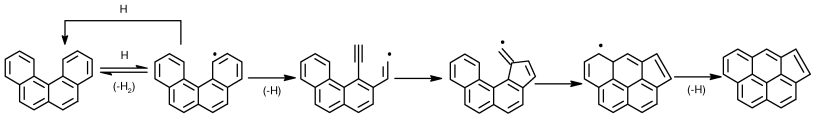	
Jump Process: 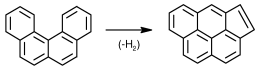	Rate: $k_{2a}\left(\frac{k_{1a}[\mathrm{H}]+k_{24}[\mathrm{OH}]}{k_{-1}[\mathrm{H_2}]+k_{25}[\mathrm{H}]+k_{-24}[\mathrm{H_2O}]+k_{2a}}\right)[\mathrm{C_{bay}R6}]$
S20 6-member ring rearrangement at bay [41] (Process 3)	**6-member ring next to bay**
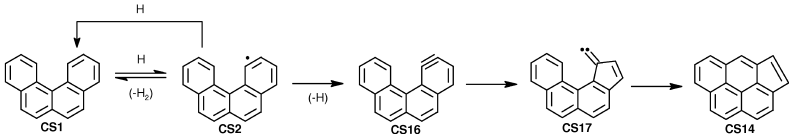	
Jump Process: 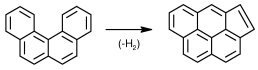	Rate: $k_{26}\left(\frac{k_{1a}[\mathrm{H}]+k_{24}[\mathrm{OH}]}{k_{-1}[\mathrm{H_2}]+k_{25}[\mathrm{H}]+k_{-24}[\mathrm{H_2O}]+k_{26}}\right)[\mathrm{C_{bay}R6}]$

In [11, 41], process 2 was studied with a different pathway. Their pathway has also been included in the PAH mechanism, and is listed as process 3 in table 2. The rates of the elementary reactions involved in the pathway of process 3 were evaluated in [41]. It can be seen in table 2 and in [30] that the pathways for the surface processes involve several intermediate species. If all the intermediate species present in the reaction mechanisms are considered, the simulation of a PAH molecule would become computationally very expensive. Therefore, those species are assumed to be in steady state [8, 16]. All the

processes can then be represented as jump processes (as shown in table 2). A detailed explanation for this assumption can be found in [8, 30]. The rate (R_i) of jump process i after steady state analysis can be represented as:

$$R_i \quad = \quad k_i \times C_s \times N_{site}, \qquad i = 1, 2 \ldots I$$

where, k_i is the process rate constant, C_s is the concentration of the chemical species involved in the bimolecular reactions, N_{site} is the number of reactive sites on the PAH molecule involved in the process, and I is the total number of processes listed in table 2 appended with the process list given in [30]. The rate expressions for the new processes obtained after a steady state analysis are given in table 2.

The stochastic algorithm developed in [30] to track the structure of PAHs after each reaction step is briefly reviewed here. The PAH growth process is modelled as a Markovian sequence of reaction events [14]. The outcome of this model depends on the concentration of chemical species, the rates of the possible process events and the probability of a reaction to be chosen. A seed molecule is required on which the surface processes can take place. In this study pyrene was chosen as the seed molecule due to its importance in soot nucleation [2]. At time t, an exponentially distributed waiting time for a process to take place, τ with parameter λ is calculated, where λ is the sum of all the jump process rates:

$$\lambda = \sum_{i=1}^{I} R_i$$

$t = t + \tau$ gives the time for the next PAH process. A jump process is chosen based on the probability calculated using its rate. A site of correct type is chosen uniformly assuming all sites to be equally probable. The PAH structure is then updated based on the chosen process and the above procedure is repeated for the desired simulation time.

5 Results and discussion

5.1 Reaction rates

The rate constants of the elementary reactions involved in the new proposed processes are listed in table 3. It is worth mentioning that the Wigner correction factor varied between 2.5 and 1 in the temperature range of 300–3000 K for all the reactions, and it remained close to 1 for T $>$ 1000 K. The rate constants for some of the elementary reactions, which are present in the rate expressions of the jump processes (in table 2), but not studied in this work, were taken from the literature. These are also provided in table 3.
One of the principal steps in processes 1 and 2 is the decyclisation of a six member ring. In [13], the rate constant for the decyclisation of phenyl radical was evaluated using the MIND0/3 parametrisation of SCF-MO theory. Two of the PAH processes proposed in [16] (6-member ring desorption and conversion of 6-member ring to 5-member ring) involved decyclisation of a 6-member ring. A rate constant for this reaction is given in their work,

but, its origin is not clear. Figure 6 provides the comparison between the rate constants for the decyclisation reaction from the literature and the rate constant evaluated in this work. A good agreement between all the rate constants was obtained, especially at high temperatures. This provides further support to the level of theory used in this work.

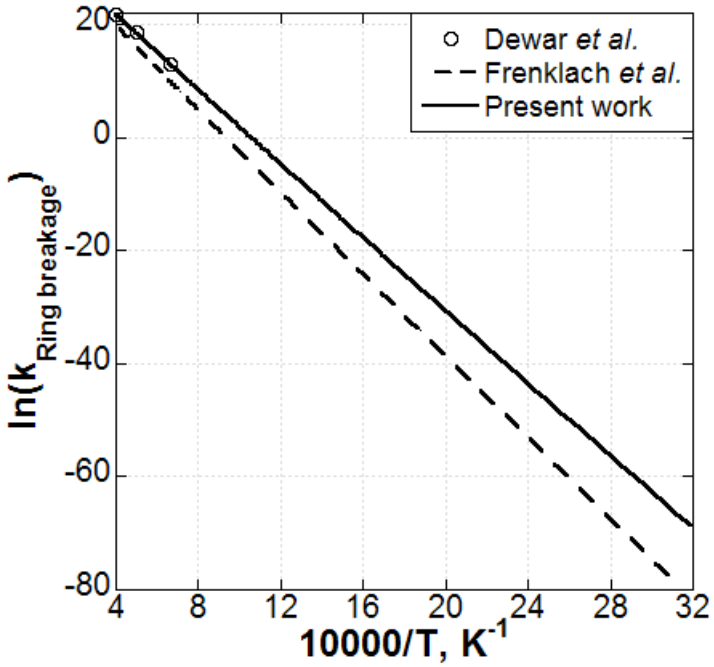

Figure 6: *Comparison of the rate constants for decyclisation of a six-member ring. Hollow circles: rate constant for the decyclisation of phenyl ring evaluated by Dewar et al. [13]. Dashed line: rate constant for 6-member ring breakage reaction used by Frenklach et al. [16]. Solid line: rate constant for the decyclisation of 6-member ring adjacent to a bay site evaluated in this work.*

Table 3: *Elementary reaction rate constants in the form:* $\mathrm{AT^n\,exp(-E/RT)}$. *The units are* $kcal$, K, mol, cm *and* sec. p.w. *represents the rate constants calculated in the present work using B3LYP/6-311++G(d,p).*

No.	Reaction	A	n	E	Ref.
Process 1					
1a	$CS1 + H \rightarrow CS2 + H_2$	7.81×10^{07}	1.772	10.33	p.w.
1b	$CS1 + H \rightarrow CS2 + H_2$	7.25×10^{07}	1.760	9.690	[41]
-1	$CS2 + H_2 \rightarrow CS1 + H$	3.40×10^{09}	0.880	7.870	p.w.
2a	$CS2 \rightarrow CS3$	2.30×10^{09}	1.6031	61.85	p.w.
2b	$CS2 \rightarrow CS3$	2.0×10^{11}	0.2	42.57	[13]
2c	$CS2 \rightarrow CS3$	1.3×10^{11}	1.08	70.48	[16]
3	$CS3 + H \rightarrow CS4$	1.32×10^{07}	1.779	0.1021	p.w.
4	$CS4 \rightarrow CS5 + C_2H_2$	2.54×10^{08}	1.818	18.55	p.w.
5	$CS5 + H \rightarrow CS6$	3.18×10^{09}	1.175	4.58	p.w.
6	$CS6 \rightarrow CS7$	1.91×10^{09}	1.138	1.629	p.w.

No.	Reaction	A	n	E	Ref.
7	$CS6 \rightarrow CS9$	1.70×10^{10}	1.091	2.936	p.w.
8	$CS7 \rightarrow CS8 + H$	1.56×10^{09}	1.204	15.31	p.w.
9	$CS9 \rightarrow CS10$	9.57×10^{09}	0.6555	2.81	p.w.
10	$CS10 \rightarrow CS8 + H$	1.37×10^{08}	1.511	28.26	p.w.
11	$CS3 \rightarrow CS3' + C_2H_2$	7.81×10^{08}	1.815	32.43	p.w.
12	$CS3' + H \rightarrow CS4'$	9.86×10^{09}	1.019	4.580	p.w.
13	$CS4' \rightarrow CS7'$	2.77×10^{09}	0.901	1.162	p.w.
14	$CS7' \rightarrow CS8'$	1.05×10^{10}	0.593	2.81	p.w.
15	$CS8' \rightarrow CS6' + H$	1.94×10^{08}	1.491	29.81	p.w.
16	$CS4' \rightarrow CS5'$	2.68×10^{10}	0.4287	2.032	p.w.
17	$CS5' \rightarrow CS6' + H$	1.60×10^{09}	1.199	15.52	p.w.
Process 2					
18	$CS3 \rightarrow CS11$	1.14×10^{08}	1.156	0.266	p.w.
19	$CS11 \rightarrow CS12$	6.77×10^{08}	1.065	0.1354	p.w.
20	$CS12 \rightarrow CS13$	2.44×10^{08}	1.007	2.046	p.w.
21	$CS13 \rightarrow CS14 + H$	6.49×10^{07}	1.731	37.58	p.w.
22	$CS11 \rightarrow CS15$	4.34×10^{08}	0.936	4.754	p.w.
23	$CS15 \rightarrow CS14 + H$	1.21×10^{08}	1.542	15.77	p.w.
Other reactions					
24	$CS1 + OH \rightarrow CS2 + H_2O$	2.10×10^{13}		4.570	[15]
-24	$CS2 + H_2O \rightarrow CS1 + OH$	3.68×10^{08}	1.139	17.10	[8]
25	$CS2 + H \rightarrow CS1$	2.18×10^{35}	-6.51	11.53	[15]
26	$CS2 \rightarrow CS16$ $(Process\ 3)$	1.23×10^{10}	1.410	85.20	[41]

5.2 KMC simulation

A literature survey was undertaken to gain an insight into the experimental data available on PAH ensembles in flame environments for the validation of the KMC-ARS model. PAHs present in a low–pressure C_6H_6 and C_2H_2 flames have been observed experimentally in [1, 23, 45] using Resonance Enhanced Multi-Photon Ionisation (REMPI) and time of flight–mass spectrometry (TOF-MS). The experimental details are provided in [1, 21]. The PAHs ensembles, observed experimentally at different HABs are represented on C-H diagrams. Such C-H diagrams are reported mostly for PAHs with less than 70 C atoms. In [30, 40], comparisons between the computed and the observed PAH ensembles in the size range of 6 to 70 C atoms were shown, and a close agreement between the two was found. For the experimentally observed PAHs larger than 70 C atoms, the information about their composition in terms of C/H ratio is provided in [45] for a C_2H_2 flame. These PAHs are present at higher heights above the burner, and their C/H ratios lie close to the peri-condensed PAHs. However, for such PAHs, no comparison between the observed and the computed PAH ensembles has been shown in the past.

In [30], the simulated concentration profiles of the chemical species present in a C_2H_2-O_2 flame (C/O = 1, cold gas velocity = 42 cm/sec, pressure = 0.0267 atm) are provided. In this work, those species profiles were used to generate, computationally, a PAH ensemble consisting of PAHs with the number of C atoms in between 70 and 320 in the C_2H_2 flame using the KMC-ARS model at HAB = 25 mm. Figure 7 presents a comparison between

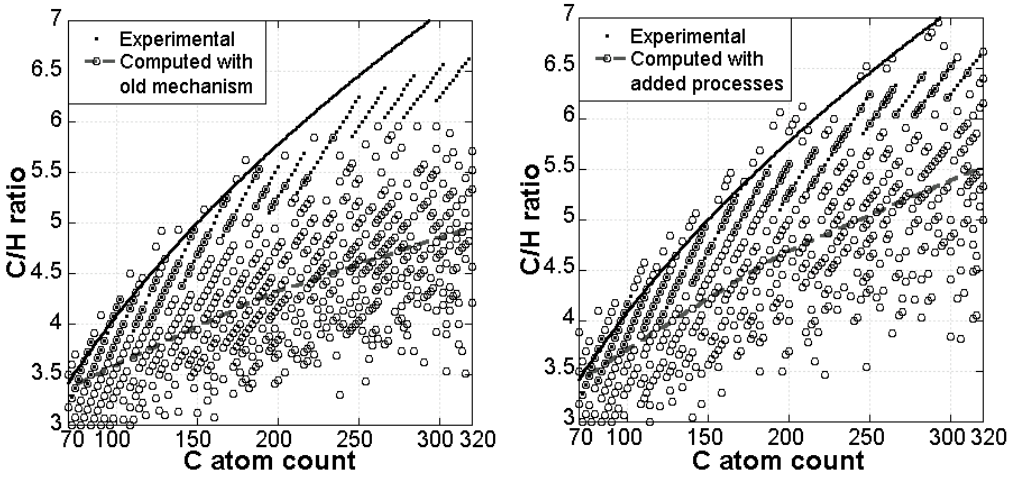

(a) (b)

Figure 7: *C/H ratio vs C atom count for large PAHs. (a) C/H ratio diagram with the PAH growth processes listed in [30] (old model); (b) C/H ratio diagram after adding the PAH processes proposed in this work to the process list of [30] (new model). The solid black lines in both the sub-figures represent the PAHs with peri-condensed rings. The dashed lines are the smooth fitted curves through the simulated data obtained using the locally weighted least squared error method.*

the simulated and the observed PAH ensembles, with and without the inclusion of the proposed PAH processes in the chemical mechanism. The simulation results obtained using the mechanism without the new PAH processes in it would be referred to as the results from the "old model", and those obtained after including the new processes in the mechanism, as the results from the "new model". The black solid lines in the sub-figures represent the positions of peri-condensed PAHs on C-H diagrams [23]. The grey broken lines in this figure are the smooth fitted curves through the simulated data obtained using the locally weighted least squared error method. Figure 8 represents the smooth fitted curves through the computed C/H ratios with and without the new PAH processes in the mechanism (shown by the black solid line and the broken line, respectively) and the experimentally observed C/H ratios of the PAHs (shown by black filled circles). The systematic errors in the simulated C/H ratios (difference between the observed and the computed C/H ratios) are also shown by corresponding grey lines. It is clear from this figure that the introduction of new PAH processes has improved the predicted C/H ratio for the large PAHs. It can be seen in figure 7 that some of the simulated PAHs have C/H ratio greater than those in peri-condensed structures (all the data points above the solid black line). This is due to the presence of 5-member rings surrounded by two to four 6-member rings on the PAHs. Some example PAHs of such kind are shown in figure 9. This figure shows a peri-condensed PAH ($C_{24}H_{12}$), and two isomers of $C_{24}H_{10}$. The C/H ratios of the $C_{24}H_{10}$ isomers are greater than the peri-condensed structure with the same number of C atoms. Such PAHs with C/H ratio greater than the peri-condensed structures can also exist if they have alkynyl side chains, which are poor in H atom content such

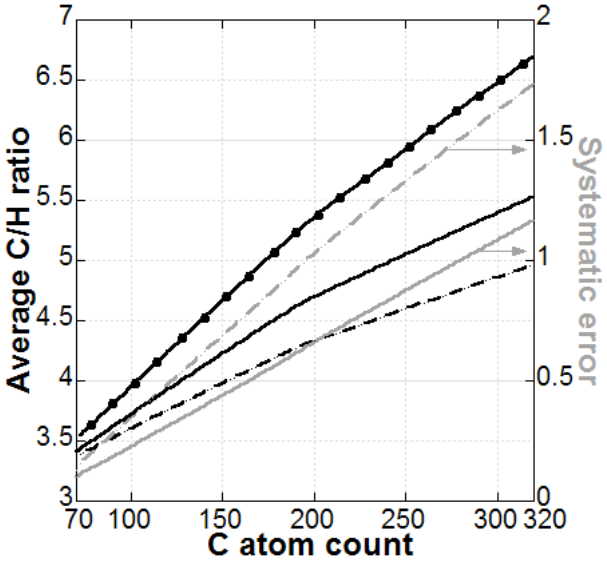

Figure 8: *Improvement in the model prediction of C/H ratio of large PAHs. The black circles represents the average C/H ratio of experimentally observed PAHs. The black solid line and the black broken line represent the average C/H ratios of computed PAHs with and without including the new PAH processes in the mechanism, respectively (also shown in figure 7). The corresponding grey lines represent the systematic errors in the computed C/H ratios.*

as C_2H chain. However, the reaction mechanism used in this work does not allow the formation of aliphatic side chains such as CH_3 and C_2H on PAHs.

For PAHs larger than 200 C atoms, the C/H ratios of the computed PAHs are significantly under-predicted. There can be three probable reasons behind it—(a) the assumption of planar or near-planar growth of PAH molecules: If an embedded 5-member ring surrounded by four 6-member rings is present on a PAH, the armchair growth reaction on it (figure 10), which can further dehydrogenate the PAHs, is not allowed in the simulation. This is because, the resulting PAH molecule would acquire a 3D geometry, and molecular dynamics would be required to determine the resulting structure, which can significantly increase the computational time. In [42], the variation in simulated C/H ratio of PAHs with PAH mass and residence time in a flame was obtained by studying the 3-dimensional growth of PAHs using kinetic Monte Carlo (KMC) and molecular dynamics (MD) methodologies. With no assumptions on the PAH structure and with a similar chemical mechanism used in [30], C/H ratio of 5 is predicted for PAHs with around 320 C atoms. This value is the same as the average predicted C/H ratio for such PAHs with the old mechanism, as shown in figure 7a. Therefore, the structural assumption in our simplified and computationally inexpensive PAH growth model may not explain the under-predicted C/H ratio. (b) the uncertainties in the rate constants: The use of incorrect process rate constants can completely change the growth pathways of PAHs, leading to the formation of H-rich PAHs. However, the uncertainties in the theoretically calculated rate constants are not known, and therefore, its effect on the computed PAH composition

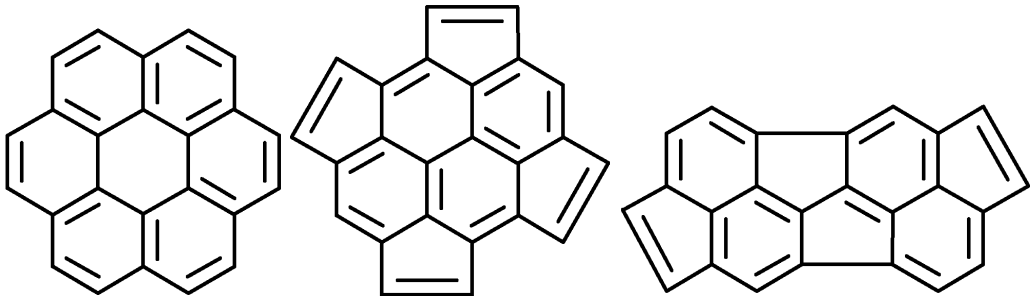

(a) $C_{24}H_{12}$ (C/H = 2) (b) $C_{24}H_{10}$ (C/H = 2.4) (c) $C_{24}H_{10}$ (C/H = 2.4)

Figure 9: *Example PAHs with the same number of C atoms. (a) represents a peri-condensed PAH. (b) and (c) represent PAHs with C/H ratio greater than the peri-condensed structure with the same number of C atoms.*

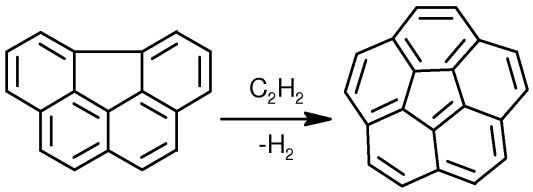

Figure 10: *Armchair growth reaction on an embedded 5-member ring surrounded by four 6-member rings.*

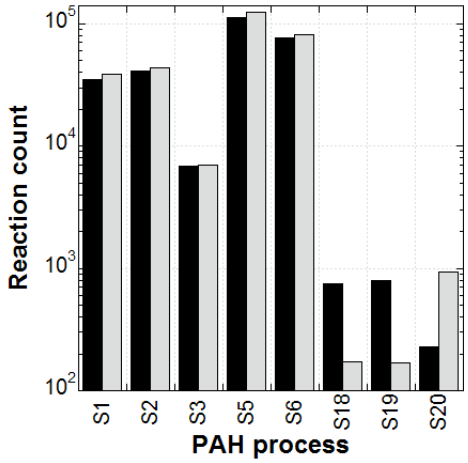

Figure 11: *Reaction counts for some of the principal PAH processes listed in [30] and table 2 (S1: Free-edge growth; S2: Armchair growth; S3: R6 desorption; S5: R5 addition; S6: R5 desorption; S18–S20: see table 2). The bars in black colour represent the reaction counts, when the PAH reaction rates are not perturbed. The bars in grey colour represent the reaction counts, when the rate constants of the reactions involved in S18 and S19 are reduced by a factor of 10.*

is difficult to determine. A further analysis on this possibility is provided later in this paper. (c) the requirement of more rearrangement processes to dehydrogenate the large PAHs: The introduction of new PAH processes in the chemical mechanism similar to the ones proposed in this work can cause further dehydrogenation of larger PAHs. It is worth mentioning that PAHs with more than 200 C atoms are not present in high concentrations in the premixed laminar aliphatic flames [20].

As mentioned previously, for process 2, a pathway different from the one proposed in this work, is suggested in [11, 42] (see process 3 in table 2). It was possible to determine the number of times, processes 2 and 3 took place on the PAH molecules in the simulation. Figure 11 shows a comparison of the number of process events that occurred on the PAHs in the environment of C_2H_2 flame in 500 simulation runs. It is clear from this figure that the pathway proposed in this work for the conversion of benzo[*c*]phenanthrene to cyclopenta[*cd*]pyrene is highly competitive with the one proposed in [11, 42]. All the three processes (S17–S19) take place at higher temperatures (T $>$ 1200 K) in the simulations.

As shown in figure 1, an under-predicted barrier height by DFT calculations can lead to an over-estimation of the rate constants by an order of magnitude (at higher temperatures). Therefore, firstly a preliminary "order of magnitude analysis" was conducted on the two proposed processes (S18 and S19) by reducing their rate constants evaluated in this work by a factor of 10, and then analysing its effect on the KMC simulation results. It can be seen in figure 11 that this reduction in rate constant significantly reduced the number of times, those processes took place on PAH molecules. In this test, the effect of rate-reduction on the counts of processes S18 and S19 is more pronounced due to the presence

of a competing process, S20, occurring on the same reactive site type, which is required by S18 and S19 to take place. The higher process rate of S20 (as compared to the reduced rates of S18 and S19) diminishes the probability of S18 and S19 to take place on a PAH, when all the three processes are competing for the same reactive site.

5.3 Sensitivity analysis

It is clear from the above analysis that the occurrence of a PAH process gets affected significantly with the variation in the rate constants of elementary reactions. Therefore, a detailed sensitivity analysis was carried out to study the effect of perturbations in the reaction rate constants on the computed C/H ratio. For all the elementary reactions present in the new model, the rate constants k_i's were varied within an order of magnitude by multiplying "perturbing factors" f_i's ranging between 0.1 and 10 to get the perturbed rate constants k_i''s:

$$k_i' = f_i \times k_i,\ 1 \leq i \leq n$$

where n is the number of elementary reactions in the PAH growth mechanism. The perturbing factors f_i's were generated using logarithmically distributed random numbers between 0.1 and 10, as explained ahead. Firstly, uniformly distributed random numbers R_i's between -1 and 1 were generated. Thereafter, the perturbing factors were calculated as:

$$f_i = 10^{R_i}$$

The purpose of generating logarithmically distributed random numbers was to achieve their uniform distribution on a log-scale in the range 0.1—10.

The perturbed rate constants were then used to evaluate the process rates in the simulation. 200 sets of perturbing factors were generated. For each set of factors, an ensemble of 200 PAH molecules was computed. The grey shaded area in figure 12 shows the range in which the average C/H ratios of the computed PAHs would lie, if the rates of the reactions present in the mechanism appended with the proposed processes (new model) are varied within an order of magnitude. All the experimental data points are present well within the shaded area. It is clear that the predicted C/H ratios can be significantly affected by varying the PAH reaction rates. A similar sensitivity analysis was carried out with the old model [30] (without the new PAH processes). In order to compare the results computed from the old and the new model, the mean values of the C/H ratios were evaluated, as shown by black and grey thin solid lines, respectively, in figure 12 (see the figure inset). Note that, to evaluate the mean, all the data points (C/H ratios) obtained for different sets of perturbing factors were used in both the cases. The standard errors on the calculated means are shown by corresponding broken lines. Clearly, the mean of the C/H ratios of the PAHs computed with the new model is closer to the experimental data than the one computed with the old model. It is worth mentioning that for all the sets of perturbing factors, the C/H ratios predicted by the new model were greater than the old model due to the presence of dehydrogenation reactions proposed in this work.

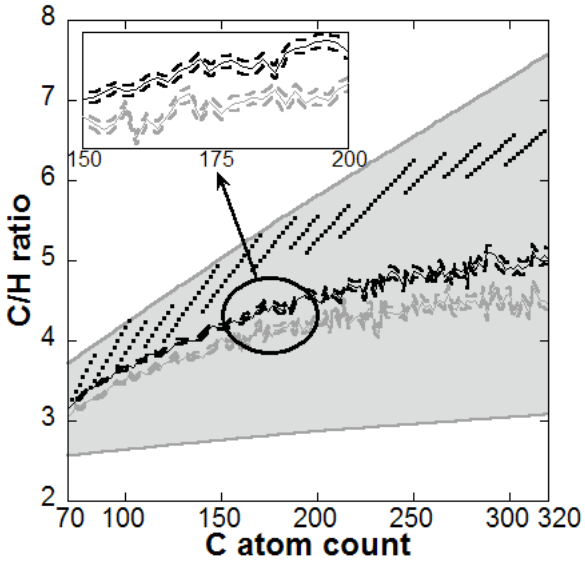

Figure 12: *Sensitivity analysis. The grey shaded area represents the range in which the average simulated C/H ratios would lie, if all the reaction rates present in the mechanism appended with the proposed processes (new model) are varied within an order of magnitude. The black circles represent the experimental data points. Solid thin black line: mean over all the simulated C/H ratios obtained using the new model (mean over the shaded area). Dashed black lines: mean ± standard error. Solid thin grey line: mean over all the simulated C/H ratios obtained with the above mentioned variation in the rates of the reactions present in the old model [30] (without the proposed processes). Dashed grey lines: mean ± standard error.*

5.3.1 Hypothesis test

In order to statistically check that no unwarranted claims have been made about the size of the difference between the two models, a hypothesis test was performed for each even numbered C atom count between 70 and 320. There are two 'populations' of C/H ratio values: $X_1, \ldots, X_p$ and $Y_1, \ldots, Y_q$ being the random variables corresponding to the PAH molecules resulting from the old and the new models respectively. A non-parametric test called the Wilcoxon (two-sample) Sum Rank test [25] was employed (it turns out that this test is equivalent to the Mann-Whitney U test). This has the following hypotheses:

$$H_0 : F_X(z) = F_Y(z) \qquad H_1 : F_X(z) > F_Y(z) \tag{4}$$

where F_X is the cumulative distribution function of X (X is the PAH population from the old model). The alternative hypothesis H_1 has the interpretation that Y has heavier tails to the right than X and thus Y tends to have larger values. Note that the form of the Wilcoxon Sum Rank test used is one which takes into account repeated values in $X_1, X_2, \ldots, X_p, Y_1, Y_2, \ldots, Y_q$. It is found that we reject the null hypothesis for 120 out of 126 carbon atom counts at the 1% significance level, whilst we reject the null hypothesis for all carbon atom counts at the 5% significance level.

These tests indicate that, regardless of the given uncertainties in the rate constants of all the PAH reactions, the inclusion of new PAH processes in the mechanism always improves the computed C/H ratios.

Additionally, the shaded area in figure 12 suggests that the predicted C/H ratios may improve if the rate constants for all the reactions are precisely measured (or calculated with a high level of DFT theory), and used in the simulation. Such quantum calculations on all the PAH reactions are beyond the scope of this paper.

6 Conclusion

This paper proposes two new PAH surface processes, which can lead to PAH dehydrogenation through ring decyclisation, followed by desorption of an alkyl chain, or rearrangement of the alkyl chains to form a 5-member ring. A new sequence of reactions for the H-mediated desorption of C_2H_2 has been suggested. Two probable routes for each process have been provided–one based on the migration of a hydrogen atom in the bay region, and the other involving bond formation between nearby C atoms in a bay region. The B3LYP functional with the 6-311++G(d,p) basis set has been used for the quantum mechanical calculations on the chemical species and the transition states involved in the pathways. The rate constants for all the elementary reactions were calculated using transition state theory (TST), and were corrected to account for quantum tunnelling using the Wigner correction method. Both the processes are highly competitive with each other. A kinetic Monte Carlo simulation of the previously proposed PAH growth model (the KMC-ARS model) in a C_2H_2 flame environment was carried out by including the new processes in the PAH growth mechanism. The proposed PAH processes improve the model prediction of the C/H ratio for large PAHs, especially, the PAHs with 70 to 200 carbon atoms. These PAH processes are required to be incorporated in the chemical mechanism of the

aromatic-site soot model [8] to improve the model predictions of the composition of soot particles in flames and engines. Furthermore, to assess the effect of inaccuracy in reaction rate constants (introduced by DFT) on KMC simulation results, a detailed sensitivity analysis has been conducted by varying the rate constants of all the reactions present in the PAH growth mechanism within an order of magnitude. A significant variation in the average C/H ratios of the computed PAHs was observed with the change in reaction rate constants.

Acknowledgement

The authors are thankful to Dr. Aron Cohen from the University Chemical Laboratory, Cambridge for the useful discussion on the use of Density Functional Theory for the quantum calculations on large molecular systems. A.R. is grateful to Cambridge Commonwealth Trusts (CCT) and Clare College, Cambridge for their financial support. The authors acknowledge the support of EPSRC under EP/C547241/1 and EP/E01724X/1.

References

[1] J. Ahrens, M. Bachmann, T. Baum, J. Griesheimer, R. Kovacs, P. Weilmünster, and K. H. Homann. Fullerenes and their ions in hydrocarbon flames. *Int. J. Mass Spectrom.*, 138:133–148, 1994.

[2] J. Appel, H. Bockhorn, and M. Frenklach. Kinetic modeling of soot formation with detailed chemistry and physics: Laminar premixed flames of C_2 hydrocarbons. *Combust. Flame*, 121:122–136, 2000. doi:10.1016/S0010-2180(99)00135-2.

[3] J. Baker, A. Scheiner, and J. Andzelm. Spin contamination in density functional theory. *Chem. Phys. Lett.*, 216:380–388, 1993.

[4] T. R. Barfknecht. Toxicology of soot. *Prog. Energy Combust. sci.*, 9:199–237, 1983.

[5] D. L. Baulch, C. T. Bowman, C. J. Cobos, R. A. Cox, T. Just, J. A. Kerr, M. J. Pilling, D. Stocker, J. Troe, W. Tsang, R. W. Walker, and J. Warnatz. Evaluated Kinetic Data for Combustion Modeling: Supplement II. *J. Phys. Chem. Ref. Data*, 34:757–1397, 2005.

[6] R. L. Bell and T. N. Truong. Direct ab initio dynamics studies of proton transfer in hydrogen-bond systems. *J. Chem. Phys.*, 101:10442–10451, 1994.

[7] M. S. Celnik, R. I. A. Patterson, M. Kraft, and W. Wagner. Coupling a stochastic soot population balance to gas-phase chemistry using operator splitting. *Combust. Flame*, 148(3):158–176, 2007. doi:10.1016/j.combustflame.2006.10.007.

[8] M. S. Celnik, A. Raj, R. H. West, R. I. A. Patterson, and M. Kraft. An aromatic site description of soot particles. *Combust. Flame*, 155(1-2):161–180, 2008. doi:doi:10.1016/j.combustflame.2008.04.011.

[9] M. S. Celnik, M. Sander, A. Raj, R. H. West, and M. Kraft. Modelling soot formation in a premixed flame using an aromatic-site soot model and an improved oxidation rate. *Proc. Combust. Inst.*, 32(1):639–646, 2009. doi:doi:10.1016/j.proci.2008.06.062.

[10] H. X. Chen and R. A. Dobbins. Crystallogenesis of Particles Formed in Hydrocarbon Combustion. *Combust. Sci. Technol.*, 159:109–128, 2000.

[11] J. Cioslowski, P. Piskorz, and D. Moncrieff. Electronic Structure Studies of 1,2-Dihydrogenation of Arenes and Rearrangement of Arynes to Annelated Cyclopentadienylidenecarbenes. *J. Am. Chem. Soc.*, 120:1695–1700, 1998.

[12] A. J. Cohen, P. Mori-Sánchez, and W. Yang. Fractional Spins and Static Correlation Error in Density Functional Theory. *J. Chem. Phys.*, 129:121104, 2008.

[13] M. J. S. Dewar, W. C. Gardiner Jr, M. Frenklach, and I. Oref. Rate Constant for Cyclization/Decyclization of the Phenyl Radical. *J. Am. Chem. Soc.*, 109:4456–4457, 1987. doi:10.1021/ja00249a005.

[14] M. Frenklach. On surface growth mechanism of soot particles. *Proc. Combust. Inst.*, 26:2285–2293, 1996. doi:10.1016/S0082-0784(96)80056-7.

[15] M. Frenklach and H. Wang. Detailed surface and gas-phase chemical kinetics of diamond deposition. *Phys. Rev. B*, 43(2):1520–1545, 1991. doi:10.1103/PhysRevB.43.1520.

[16] M. Frenklach, C. A. Schuetz, and J. Ping. Migration mechanism of aromatic-edge growth. *Proc. Combust. Inst.*, 30:1389–1396, 2005. doi:10.1016/j.proci.2004.07.048.

[17] M. J. Frisch, G. W. Trucks, H. B. Schlegel, G. E. Scuseria, M. A. Robb, J. R. Cheeseman, J. A. Montgomery, Jr., T. Vreven, K. N. Kudin, J. C. Burant, J. M. Millam, S. S. Iyengar, J. Tomasi, V. Barone, B. Mennucci, M. Cossi, G. Scalmani, N. Rega, G. A. Petersson, H. Nakatsuji, M. Hada, M. Ehara, K. Toyota, R. Fukuda, J. Hasegawa, M. Ishida, T. Nakajima, Y. Honda, O. Kitao, H. Nakai, M. Klene, X. Li, J. E. Knox, H. P. Hratchian, J. B. Cross, V. Bakken, C. Adamo, J. Jaramillo, R. Gomperts, R. E. Stratmann, O. Yazyev, A. J. Austin, R. Cammi, C. Pomelli, J. W. Ochterski, P. Y. Ayala, K. Morokuma, G. A. Voth, P. Salvador, J. J. Dannenberg, V. G. Zakrzewski, S. Dapprich, A. D. Daniels, M. C. Strain, O. Farkas, D. K. Malick, A. D. Rabuck, K. Raghavachari, J. B. Foresman, J. V. Ortiz, Q. Cui, A. G. Baboul, S. Clifford, J. Cioslowski, B. B. Stefanov, G. Liu, A. Liashenko, P. Piskorz, I. Komaromi, R. L. Martin, D. J. Fox, T. Keith, M. A. Al-Laham, C. Y. Peng, A. Nanayakkara, M. Challacombe, P. M. W. Gill, B. Johnson, W. Chen, M. W. Wong, C. Gonzalez, , and J. A. Pople. *Gaussian 03*, Revision E.01; Gaussian, Inc., Wallingford CT. 2004.

[18] A. G-Lafont, T. N. Truong, and D. G. Truhlar. Direct Dynamics Calculations with Neglect of Diatomic Differential Overlap Molecular Orbltai Theory with Specific Reaction Parameters. *J. Phys. Chem.*, 95:4618–4627, 1991.

[19] L. A. Gribov, I. A. Novakov, A. I. Pavlyuchko, and E. V. Vasilev. Spectroscopic calculations of CH bond dissociation energy in the series of chloro derivatives of methane, ethane and propane. *J. Struct. Chem.*, 47:635–641, 2006.

[20] J. Happold, H.-H. Grotheer, and M. Aigner. Distinction of gaseous soot precursor molecules and soot precursor particles through photoionization mass spectroscopy. *Rapid Commun. Mass Sp.*, 21:1247–1254, 2007. doi:10.1002/rcm.2955.

[21] K. H. Homann. Fullerenes and Soot Formation–New Pathways to Large Particles in Flames. *Angew. Chem.*, 37:2434–2451, 1998.

[22] T. Ishiguro, Y. Takatori, and K. Akihama. Microstructure of Diesel Soot Particles Probed by Electron Microscopy: First Observation of Inner Core and Outer Shell. *Combust. Flame*, 108:231–234, 1997. doi:10.1016/S0010-2180(96)00206-4.

[23] A. Keller, R. Kovacs, and K. H. Homann. Large molecules, ions, radicals and small soot particles in fuel rich hydrocarbon flames. *Phys. Chem. Chem. Phys.*, 2:1667–1675, 2000.

[24] V. V. Kislov, N. I. Islamova, A. M. Kolker, S. H. Lin, and A. M. Mebel. Hydrogen Abstraction Acetylene Addition and Diels-Alder Mechanisms of PAH Formation: A Detailed Study Using First Principles Calculations. *J. Chem. Theory Comput.*, 1: 908–924, 2005. doi:10.1021/ct0500491.

[25] P. H. Kvam and B. Vidakovic. *Nonparametric Statistics with Applications to Science and Engineering*. John Wiley & Sons Inc., 2007. ISBN 978-0470081471.

[26] D. R. Lide. *CRC handbook of chemistry and physics: a ready-reference book of chemical and physical data*. CRC Press, 2008. ISBN 9781420066791.

[27] J. A. Litwinowicz, D. E. Ewing, S. Jurisevic, and M. J. Manka. Transition State Structure and Properties of Hydrogen Transfer Reactions of Hydrocarbons: Ab Initio Benchmark Calculations. *J. Phys. Chem.*, 24:9709–9716, 1995. doi:10.1021/j100024a011.

[28] A. M. Mebel, M. C. Lin, T. Yu, and K. Morokuma. Theoretical Study of Potential Energy Surface and Thermal Rate Constants for the $C_6H_5 + H_2$ and $C_6H_6 + H$ Reactions. *J. Phys. Chem. A*, 101:3189–3196, 1997. doi:10.1021/jp9702356.

[29] R. I. A. Patterson and M. Kraft. Models for the aggregate structure of soot particles. *Combust. Flame*, 151:160–172, 2007. doi:10.1016/j.combustflame.2007.04.012.

[30] A. Raj, M. Celnik, R. Shirley, M. Sander, R. Patterson, R. West, and M. Kraft. A statistical approach to develop a detailed soot growth model using PAH characteristics. *Combust. Flame*, 156:896–913, 2009. doi:10.1016/j.combustflame.2009.01.005.

[31] M. Sander, A. Raj, O. Inderwildi, M. Kraft, S. Kureti, and H. Bockhorn. The simultaneous reduction of nitric oxide and soot in emissions from diesel engines. *Carbon*, 47:866–875, 2009.

[32] T. M. Selden, A. S. Forrest, and J. E. Lockhart. Analyzing the Reductions in U.S. Air Pollution Emissions: 1970 to 1990. *Land Economics*, 75:1–21, 1999.

[33] J. Singh, M. Balthasar, M. Kraft, and W. Wagner. Stochastic modelling of soot particle size and age distribution in laminar premixed flames. *Proc. Combust. Inst.*, 30:1457–1465, 2005. doi:10.1016/j.proci.2004.08.120.

[34] J. Singh, R. I. A. Patterson, M. Kraft, and H. Wang. Numerical simulation and sensitivity analysis of detailed soot particle size distribution in laminar premixed ethylene flames. *Combust. Flame*, 145:117–127, 2006. doi:10.1016/j.combustflame.2005.11.003.

[35] B. Temelso, C. D. Sherrill, R. C. Merkle, and R. A. Freitas Jr. High-Level ab Initio Studies of Hydrogen Abstraction from Prototype Hydrocarbon Systems. *J. phys. Chem. A*, 110:11160–11173, 2006.

[36] B. V. Unterreiner, M. Sierka, and R. Ahlrichs. Reaction pathways for growth of polycyclic aromatic hydrocarbons under combustion conditions, a DFT study. *Phys. Chem. Chem. Phys.*, 6:4377–4384, 2004.

[37] R. L. Vander Wal. A TEM Methodology for the Study of Soot Particle Structure. *Combust. Sci. Tech.*, 126:333–357, 1997.

[38] R. L. Vander Wal. An Illustration of Soot Structure by Dark Field Transmission Electron Microscopy. *Combust. Sci. Tech.*, 132:315–323, 1998.

[39] R. L. Vander Wal, A. Yezerets, N. W. Currier, D. H. Kim, and C. M. Wang. HRTEM Study of diesel soot collected from diesel particulate filters. *Carbon*, 45:70–77, 2007. doi:10.1016/j.carbon.2006.08.005.

[40] A. Violi. Modeling of soot particle inception in aromatic and aliphatic premixed flames. *Combust. Flame*, 139:279–287, 2004. doi:10.1016/j.combustflame.2004.08.013.

[41] A. Violi. Cyclodehydrogenation Reactions to Cyclopentafused Polycyclic Aromatic Hydrocarbons. *J. Phys. Chem. A*, 109:7781–7787, 2005. doi:10.1021/jp052384r.

[42] A. Violi, G. A. Voth, and A. F. Sarofim. The relative roles of acetylene and aromatic precursors during particle inception. *Proc. Combust. Inst.*, 30:1343–1351, 2005. doi:10.1016/j.proci.2004.08.226.

[43] H. Wang and M. Frenklach. Calculations of rate coefficients for the chemically activated reactions of acetylene with vinylic and aromatic radicals. *J. Phys. Chem.*, 98(44):11465–11489, 1994. doi:10.1021/j100095a033.

[44] H. Wang and M. Frenklach. A detailed kinetic modeling study of aromatic formation in laminar premixed acetylene and ethylene flames. *Combust. Flame*, 110:173–221, 1997. doi:10.1016/S0010-2180(97)00068-0.

[45] P. Weilmünster, A. Keller, and K. H. Homann. Large Molecules, Radicals, Ions, and Small Soot Particles in Fuel-Rich Hydrocarbon Flames Part I: Positive Ions of Polycyclic Aromatic Hydrocarbons (PAH) in Low-Pressure Premixed Flames of Acetylene and Oxygen. *Combust. Flame*, 116:62–83, 1999. doi:10.1016/S0010-2180(98)00049-2.

[46] R. Whitesides, A. C. Kollas, D. Domin, W. A. Lester Jr, and M. Frenklach. Graphene Layer Growth: Collision of migrating five-member rings. *Proc. Combust. Inst.*, 31: 539–546, 2007.

[47] R. Whitesides, D. Domin, R. S-Ferrer, W. A. Lester Jr, and M. Frenklach. Graphene Layer Growth Chemistry: Five- and Six-Member Ring Flip Reaction. *J. Phys. Chem. A*, 112:2125–2130, 2008.

[48] T. Wu, H.-J. Werner, and U. Manthe. First-Principles Theory for the $H + CH_4 \rightarrow H_2 + CH_3$ Reaction. *Science*, 306:2227–2229, 2004.

[49] D. C. Young. *Computational Chemistry: A Practical Guide for Applying Techniques to Real-World Problems*. John Wiley & Sons Inc., 2001.

[50] Y. Zhao and D. G. Truhlar. Density Functional for Spectroscopy: No Long-Range Self-Interaction Error, Good Performance for Rydberg and Charge-Transfer States, and Better Performance on Average than B3LYP for Ground States. *J . Phys. Chem. A*, 110(49):13126–13130, 2006.